Closed-Line Integral Optimization Edge Detection Algorithm and Its Application in Equilibrium Radionuclide Angiocardiography

Mikael Ekman, Milan Lomsky, Sven Olof Strömblad and Sten Carlsson

Departments of Radiation Physics, Clinical Physiology and Cardiology, Sahlgrenska University Hospital, Göteborg, Sweden

Automatic evaluation of left ventricular (LV) function using equilibrium radionuclide angiocardiography requires an edge detection algorithm to correct and reproducibly delineate the left ventricle. Available algorithms, usually based on differentiation of a radial profile, generally suffer from low precision due to low signal-to-noise ratios and overlapping structures, for example, the left atrium. **Methods:** An edge detection algorithm was developed based on the assumption that the LV border can be defined as the maximum, normalized, closed-line integral of a closed curve in a vector field derived by image differentiation. It is further assumed that the closed curve can be described by a Fourier expansion with a limited number of harmonics. Regions of interest (ROIs) generated by this algorithm were compared with ROIs generated by an algorithm based on a combination of thresholding and second-order derivatives. **Results:** This algorithm delineates the left ventricle and gives results more closely related to ROIs generated manually than the algorithm combining thresholding and the second-order derivative. Our algorithm can also handle the problem of overlapping structures, as demonstrated in phantom simulations. **Conclusion:** The concept of a maximum, normalized closed-line integral will improve the delineation of the LV in an equilibrium radionuclide angiocardiography study. The problem of overlapping structures is overcome by this algorithm because it takes into consideration global edge information.

Key Words: edge detection algorithms; left ventricle; equilibrium radionuclide angiocardiography

J Nucl Med 1995; 36:1014–1018

Equilibrium radionuclide angiocardiography is an important clinical and research tool for the evaluation of left ventricular (LV) heart function and has become the gold standard in prognostic studies in patients with LV dysfunction (*1*). It has been used in studies in which the values from global and regional LV functions are used to assess the value of different metabolic and perfusion imaging techniques to identify hibernating myocardium (*2*) and to monitor heart function during the treatment of cancer patients with cardiotoxic cytostatica (*3*). Equilibrium radionuclide angiocardiography is also used for risk assessment in patients with coronary heart disease (*1,4*), for assessment of thrombolytic therapy in patients with acute myocardial infarction (*5,6*) and for the assessment of other therapeutic interventions (*5,7*).

Correct and reproducible measurements of LV function, in terms of parameters such as the global and regional ejection fraction, require an accurate and reproducible algorithm to delineate the left ventricle (*8,9*). Delineation can be accomplished manually or automatically using an edge detection algorithm (EDA). The manual algorithm usually suffers from low reproducibility, whereas automatic algorithms suffer from low precision due to nonuniform background, low signal-to-noise ratios (SNR) and the complicated structure of the heart, which may result in an image with the right ventricle and left atrium overlapping the left ventricle.

The most commonly used EDA is based on the assumption that the LV border ventricle coincides with the zero crossing of the second-order derivative in a radial search with its origin in the left ventricle (*10*). To limit the search, the method is often combined with thresholding (*11*). The EDA based on combined thresholding and the second-order derivative is referred to here as the thresholding/derivative EDA. A linear combination of first- and second-order derivatives has also been suggested (*12*). Also, Reiber et al. used an algorithm based on a minimal cost function (*13*).

The aim of this study was to develop an EDA which is capable of handling the problems of low SNR and overlapping structures in the image. We have used the concept of closed-line, integral optimization. The regions of interest (ROIs) generated by our algorithm were compared with the ROIs generated by a thresholding/derivative EDA and with manually-defined ROIs. The comparison was performed on both software phantom images and images from patient studies.

MATERIALS AND METHOD

Basic Principle of the Algorithm

The algorithm is based on the hypothesis that the border of the LV ROI is defined as the closed curve which gives the maximum

Received Jul. 18, 1994; revision accepted Nov. 10, 1994.

For correspondence or reprints contact: Mikael Ekman, MSc Department of Radiation Physics, Sahlgrenska University Hospital, S-413 45 Göteborg, Sweden.

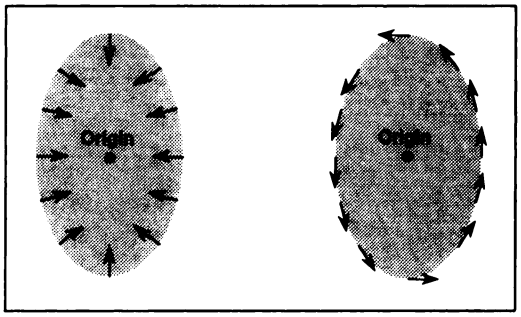

FIGURE 1. The vectors defined by differentiation of the image (left) are rotated through 90°, resulting in vectors pointing along the edge (right).

of the length-normalized, closed-line integral in a vector field derived by differentiation of the image. It further assumes that the closed curve can be described by Fourier expansion with a limited number of harmonics. In simple terms, the normalized, closed-line integral of an outline can be regarded as the sum of the slopes perpendicular to the outline at different points along the outline. It is then normalized according to the length of the curve to prevent wide outlines from being favored. The problem is then to find the closed curve which gives the maximum value of the normalized, closed-line integral.

Description of the Algorithm

A complete mathematical description of this EDA algorithm is given in the Appendix.

After selecting an origin inside the left ventricle, the image is differentiated in the radial and tangential directions for each pixel. The radial and tangential components define a vector describing the local change in count density, both in direction and magnitude. All vectors in the image are rotated through 90°, resulting in a vector field pointing along the (local) edges (Fig. 1). The closed object curve is described by Fourier expansion. The simplest curves (zero harmonics) will give a circle, while a more complex shape requires more harmonics.

Thus, the problem of finding an outline is reduced to finding the curve, i.e., the coefficients in the Fourier expansion that optimize the normalized, closed-line integral for a given number of harmonics. We used a numerical min/max algorithm, Simplex downhill (*14*).

Software Phantom

The software phantom contained an ellipsoid simulating the left ventricle with a 28-pixel long axis and a 16-pixel short axis in a 64 × 64 matrix. The left atrium was simulated by a sphere with a diameter of 14 pixels. The simulated left ventricle, left atrium was placed in a homogeneous background of 100 counts/pixel. The maximum net counts were 100 per pixel for the simulated left ventricle and 75 per pixel for the simulated left atrium. The simulated images were convoluted with the gamma camera's point spread function and finally Gaussian noise was added. Before analysis, a common, nine-point smooth was applied to the image to simulate a routine evaluation of a patient study.

Ten images with varying distances between the simulated left ventricle and left atrium were generated, starting with a separation of 2 pixels and ending with an overlap of 3 pixels (see also Fig. 2).

Patient Studies

Five patient studies (S1–S5) were selected from routine examinations. The studies were carefully chosen to represent the most commonly encountered problems when trying to correctly delineate the left ventricle using an automatic EDA. Below follows a brief characterization of the studies:

- S1: Fair separation of the left ventricle and left atrium; the edge of the left ventricle towards the left atrium is poorly defined. Slight dilatation of the left ventricle with severe anteroseptal hypokinesia and apical dyskinesia. Normal right ventricle dimensions and wall motion.
- S2: Good separation of the left ventricle and left atrium as well as the left ventricle and right ventricle. Moderate dilatation of the left ventricle with an elliptical shape, severe anteroseptal hypokinesia and apical akinesia. Normal right ventricle dimensions and wall motion.
- S3: Good separation of the left ventricle and left atrium, moderate overlapping of the left ventricle and right ventricle apex; otherwise good separation of the left ventricle and right ventricle. Normal left ventricle and right ventricle dimensions and wall motion.
- S4: Fair separation of the left ventricle and left atrium as well as the left ventricle and right ventricle. Slight dilatation of the left ventricle with a spherical shape and moderate anteroseptal and slight posterolateral hypokinesia. Normal right ventricle dimension and wall motion.
- S5: Good separation of the left ventricle and left atrium as well as the left ventricle and right ventricle. Normal left ventricle and right ventricle dimensions and wall motion.

Red blood cells were labeled with 925 MBq ^{99m}Tc using a standard in vivo/in vitro labeling procedure. Imaging was performed with an Elscint Apex 415 gamma camera system (Haifa, Israel) with the patient in the supine position. Images were recorded in the LAO projection, with a 20° caudal tilt, to give the best separation of the right and left ventricles. Data were collected in a 64 × 64 matrix using 18–32 frames per cardiac cycle and with an ECG gate tolerance of ±10%. Extrasystolic and postextrasystolic cycles were excluded. Acquisition was stopped when the left ventricular ROI contained approximately 150 counts per pixel. All studies were preprocessed with a nine-point smoothing filter prior to edge detection.

Evaluation of the Algorithm

Phantom Studies. ROIs generated by the thresholding derivative EDA (Elscint SP-1) and closed-line, integral EDA were evaluated visually with respect to their ability to exclude the nonoverlapping part of the left atrium.

Patient Studies. In each patient study, two experienced observers, independently of each other, manually defined the left ventricle in nine frames representing different phases of the cardiac cycle. Differences between the two observers were resolved by consensus, in that a consensus ROI was created as a compromise acceptable to both observers.

The 45 manual ROIs were then compared with the ROIs automatically generated by the thresholding/derivative EDA (Elscint SP-1) and the closed-line, integral EDA (using 3, 4, 5 and 6 harmonics).

The left ventricle was divided into five sectors using the geometric center of the manual ROI as the origin. The apical and outflow sectors had an aperture of 60°, the anteroseptal and posterolateral sectors had an aperture of 120° and the global sector had an aperture of 360°. The automatic and manual ROIs were compared as follows: the average radius for each ROI was determined in every sector; the difference in the average radius be-

FIGURE 2. Phantom simulation of the left atrium and the left ventricle shows frame numbers 1 (top left), 2 (top right), 9 (low left) and 10 (low right). Frame 1 shows correct delineation by both methods. Frames 2, 9 and 10 show incorrect delineation of the left ventricle with the inclusion of the left atrium by the thresholding/derivative EDA and correct delineation by the closed-line, integral EDA.

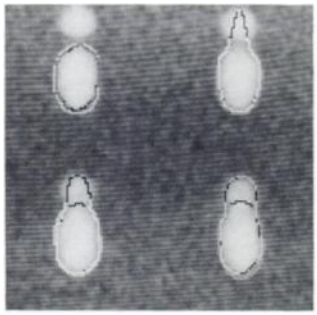

FIGURE 3. An early systolic image from study 3. Correct delineation of the left ventricle by the closed-line, integral EDA. Incorrect delineation of the left ventricle by the thresholding/derivative EDA with the inclusion of the apex of the right ventricle.

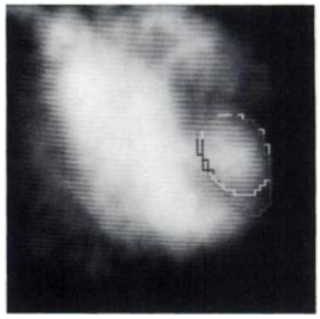

tween thresholding/derivative EDA ROIs and the manual ROIs was determined in every sector, as was the difference in the average radius between closed-line integral-EDA ROIs and the manual ROIs; and the average difference and its standard deviation were determined for each sector.

RESULTS

Phantom Studies

The thresholding/derivative EDA was successful in 2 of 10 images (images 1 and 3) and failed to exclude the nonoverlapping part of the left atrium in 8 images (Fig. 2). The closed-line integral EDA, using four harmonics, was successful in all images (Fig. 2).

Patient Studies

The differences between manual and automatic ROIs are shown in Table 1. The closed-line integral EDA generates an outline that is closer to the standard than the thresholding/derivative EDA. The closed-line, integral EDA also resulted in a slightly lower standard deviation of the differences than the thresholding/derivative EDA. The Wilcoxon signed range test shows a statistically significant difference ($p < 0.01$) between the closed-line integral EDA and the thresholding/derivative EDA in all sectors. Examples of ROIs from two patient studies are shown in Figures 3, 4 and 5.

DISCUSSION

A fully automated EDA to delineate organs is of great importance in quantitative examinations using nuclear medicine. It reduces both inter- and intraobserver variability. Several algorithms are available, ranging from thresholding to more advanced cost function analysis. The general drawbacks of simple algorithms are their sensitivity to noise and their inability to include cold spots at the edge of the organ or exclude overlapping structures.

The algorithm based on the maximum, closed-line integral described in this article generates ROIs which are significantly better than those resulting from a commonly used algorithm based on the second-order derivative when compared with ROIs manually defined by two experienced observers. Our algorithm has an inherent ability to handle the problem of overlapping organs, as shown in both software phantom experiments and in patient studies. One reason for this is the assumption that the left ventricle ROI can be described by a Fourier expansion with a limited number of harmonics, thus giving a robustness to the search for the best closed curve. Another reason is that the algorithm takes into account not only the information on the local edge but also the information of the whole ROI. The fact that the closed-line, integral EDA excludes convex parts of the count density when generating the vector field, together with the use of a limited number of harmon-

TABLE 1
Radii Differences between EDAs and Manually Drawn ROIs

	Difference (pix)					Standard deviation (pix)					
	CLI					CLI					
Section	H = 3	H = 4	H = 5	H = 6	TSD	H = 3	H = 4	H = 5	H = 6	TSD	p(Wx)
Glob	−0.23	−0.11	−0.10	−0.08	−0.41	0.47	0.49	0.48	0.46	0.49	<0.01
Sept	−0.19	−0.23	−0.20	−0.16	0.12	0.51	0.53	0.51	0.52	0.60	<0.01
Apic*	−0.16	0.20	0.33	0.42	−1.27	0.86	0.70	0.69	0.64	0.91	<0.01
Lat	−0.06	−0.14	−0.19	−0.12	−0.85	0.55	0.61	0.57	0.61	0.65	<0.01
Out	−0.62	−0.07	−0.06	−0.02	0.53	1.30	1.12	1.17	1.18	1.12	<0.01

*Thresholding/derivative EDA and closed-line, integral EDA (H = 6) failed in this region in one study. Results are based on 36 images.

The closed-line integral EDA was evaluated using 3, 4, 5, and 6 harmonics (H). Glob = globally, Sept = anteroseptal, Apic = apical, Lat = posterolateral; Out = outflow; CLI = closed-line integral; TSD = thresholding derivative. The Wilcoxon signed range test, p(Wx), was applied to closed-line, integral EDA H = 4 versus thresholding/derivative EDA. Data are based on 45 ROIs unless otherwise stated.

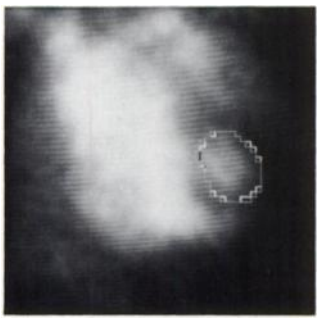

FIGURE 4. End-systolic image from study 3. Correct delineation by both methods.

ics in the Fourier expansion, makes its outlines wider and thus, closer to manually-produced ROIs.

A similar approach to edge detection algorithms has been used by Reiber et al. (*13*). The main difference is that our algorithm is based on closed-line, integral optimization, thus taking into account information concerning the direction of the (local) edge. Parametrization in outlining the left ventricle in equilibrium radionuclide angiocardiography studies using the Fourier expansion has been studied by Hosoba et al. (*9*), who found six harmonics to be the optimal choice in describing LV contour. Our results indicate that a lower number of harmonics is sufficient.

The major drawback of our algorithm is its computational complexity. With the gamma camera computer system (Elscint SP-1) used in this study, the closed-line integral EDA takes about 30 sec per image. By using modern workstations, however, this time can be reduced significantly. There is reason to believe that algorithms using global edge information, as in the case with closed-line, integral evaluation, are less noise-sensitive than algorithms using local edge information.

Future work will include the reduction of the standard deviation in the differences between ROIs generated by closed-line, integral EDA and manually-defined reference ROIs. The most crucial step seems to be the numerical min/max algorithm. Other min/max algorithms will also be considered.

CONCLUSION

Our algorithm improves delineation of the left ventricle in an equilibrium radionuclide angiocardiography study because it applies both local as well as global edge information.

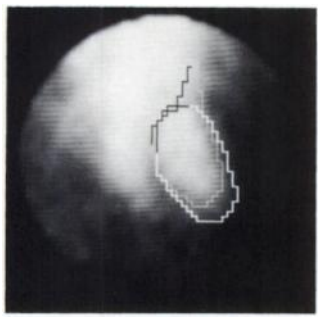

FIGURE 5. Late systolic image from study 1. Correct delineation of the left ventricle by the closed-line, integral EDA. The thresholding/derivative EDA excludes the apex of the left ventricle and includes part of the left atrium. The upper border of the thresholding/derivative EDA ROI differs by only 1 pixel from the diastolic reference ROI and thus lies within the mask ROI.

APPENDIX

Polar Coordinate System Definition

The image is described in polar coordinates $I(r, \phi)$. This requires the definition of an origin which is assumed to be anywhere inside the object being outlined.

Parametrization of the Closed Curve

The closed curve is defined by the radius which is a function of angle $L(\phi)$. It is assumed that there is 1:1 mapping between angle and radius. The parametrization is performed by Fourier expansion

$$L(\phi) = \frac{a_0}{2} + \sum_{i=1}^{H} (a_i \cos(\phi * i) + b_i \sin(\phi * i)), \qquad \text{Eq. A1}$$

where H is the number of harmonics used. Before performing closed-line integration, the curve derivative must be evaluated:

$$\vec{T}(\phi) = \frac{dL(\phi)}{d\phi}\hat{r} + L(\phi)\hat{\phi}. \qquad \text{Eq. A2}$$

As can be seen, the curved derivative is represented as a vector and is interpreted as the movement indicated by the tangent of the curve per unit step in ϕ.

Image Differentiation and Creating the Vector Field

The image is differentiated in both the radial and tangential directions by applying the gradient operator to the image. This forms a vector field pointing along the gradient, perpendicular to the local edges.

$$\nabla I(r, \phi) = \frac{\partial I(r, \phi)}{\partial r}\hat{r} + \frac{1}{r}\frac{\partial I(r, \phi)}{\partial \phi}\hat{\phi}. \qquad \text{Eq. A3}$$

To avoid too tight a delineation, all gradients originating from the convex parts of the count density are excluded:

$$\nabla I(r, \phi) = \vec{0} \quad \text{if} \quad \left(\frac{\partial^2 I(r, \phi)}{\partial r^2} < 0.0\right) \quad \text{or} \quad \left(\frac{\partial^2 I(r, \phi)}{\partial \phi^2} < 0.0\right) \qquad \text{Eq. A4}$$

$$\nabla I(r, \phi) = \nabla I(r, \phi) \quad \text{otherwise.}$$

To make this vector field point along the edges in the counterclockwise direction, the vectors are rotated using the rotation operator **R**:

$$\nabla I(r, \phi)_R = \nabla I(r, \phi)\mathbf{R}, \qquad \text{Eq. A5}$$

where $\mathbf{R} = \begin{bmatrix} 0 & 1 \\ -1 & 0 \end{bmatrix}$.

Criteria for Optimizing Normalized Closed-Line Integrals

The normalized, closed-line integral is defined by the following equation:

$$\oint_{L(\phi)} \nabla I(r, \phi)_R \cdot \frac{\vec{T}(\phi)}{|\vec{T}(\phi)|}\, d\phi. \qquad \text{Eq. A6}$$

The integral is a scalar product between the vector field generated by the gradient operator, and the derivative of the closed curve.

The derivative of the curve is normalized to achieve a result which is independent of curve length.

REFERENCES

1. Miller TD, Taliercio CP, Zinsmeister AR, Gibbons RJ. Risk stratification of single or double vessel coronary artery disease and impaired left ventricular function using exercise radionuclide angiography. *Am J Cardiol* 1990;65: 1317–1321.
2. Ragosta M, Beller GA, Watson DD, Kaul S, Gimple LW. Quantitative planar rest-redistribution Tl-201 imaging in detection of myocardial viability and prediction of improvement in left ventricular function after coronary bypass surgery in patients with severely depressed left ventricular function. *Circulation* 1993;87:1630–1641.
3. Alexander J, Dainiak N, Berger HJ, et al. Serial assessment of doxorubicin cardiotoxicity in quantitative radionuclide angiocardiography. *N Engl J Med* 1979;300:278–283.
4. Multicenter Postinfarction Research Group. Risk stratification and survival after myocardial infarction. *N Engl J Med* 1983;309:331–336.
5. Sheeman F, Braunwald E, Canner P, et al. The effect of intravenous thrombolytic therapy on left ventricular function: a report on tissue-type plasminogen activator and streptokinase from the thrombolysis in myocardial infarction (TIMI phase I) trial. *Circulation* 1987;75:817–829.
6. White HD, Norris RM, Brown MA, et al. The effect of intravenous streptokinase on left ventricular function and early survival after acute myocardial infarction. *N Engl J Med* 1987;317:850–855.
7. Andersson B, Lomsky M, Waagstein F. The link between acute haemodynamic adrenergic beta-blockad and long-term effects in patients with heart failure. *Eur Heart J* 1993;14:1375–1385.
8. Jackson PC. Evaluating the performance of an edge detection algorithm for use in radioisotope imaging. *Phys Med Biol* 1982;27:No 8:1045–1055.
9. Hosoba M, Wani H, Hiroe M, Kusakabe K. Clinical validation of fully automated contour detection for gated radionuclide ventriculography with a slant hole collimator. *Eur J Nucl Med* 1986;12:53–59.
10. Reiber Johan HC. Quantitative analysis of left ventricular function from equilibrium gated blood pool scintigrams: an overview of computer methods. *Eur J Nucl Med* 1985;10:97–110.
11. Bingham J, Okada R, McKusick K, Boucher C, Tarolli E, Alpert N, Strauss W. Comparison of three semiautomatic methods for determination of left ventricular ejection fraction from gated cardiac blood pool images. *Eur J Nucl Med* 1985;10:494–499.
12. Reiber Johan HC. Quantitative analysis of left ventricular function from equilibrium gated blood pool scintigrams: an overview of computer methods. *Eur J Nucl Med* 1985;10:97–110.
13. Reiber Johan HC, Lie SP, Hoek C, Gerbrands JJ, Wijns W, Bakker WH, Kooij Peter PM. Clinical validation of fully automated computation of ejection fraction from gated equilibrium blood pool scintigrams. *J Nucl Med* 1983;24:1099–1107.
14. Press HW, Flannery PB, Teokolsky AS, Vetterling TW. *Numerical recipes in Pascal*. Cambridge, MA: Cambridge University Press, 1986.